Defect motion and lattice pinning barriers in Josephson-junction ladders

H. Kang,[1] Jong Soo Lim,[1] J.-Y. Fortin,[2] J. Choi,[3] and M. Y. Choi[1,4]
[1]*Department of Physics and Center for Theoretical Physics, Seoul National University, Seoul 151-747, Korea*
[2]*Laboratoire de Physique Théorique, Université Louis Pasteur, 67084 Strasbourg, France*
[3]*Department of Physics, Keimyung University, Daegu 704-701, Korea*
[4]*Korea Institute for Advanced Study, Seoul 130-722, Korea*
(Received 7 September 2005; published 6 January 2006)

We study the motion of domain wall defects in a fully frustrated Josephson-junction ladder system, driven by small applied currents. For small system sizes, the energy barrier E_B to the defect motion is computed analytically via symmetry and topological considerations. More generally, we perform numerical simulations directly on the equations of motion, based on the resistively-shunted junction model, to study the dynamics of defects, varying the system size. Coherent motion of domain walls is observed for large system sizes. In the thermodynamical limit, we find $E_B=0.1827$ in units of the Josephson coupling energy.

DOI: 10.1103/PhysRevB.73.014504 PACS number(s): 74.50.+r, 03.75.Lm, 74.81.Fa, 74.25.Qt

I. INTRODUCTION

Two-dimensional (2D) arrays of Josephson junctions are of interest in various fields of fundamental classical and quantum physics. In the simplest case, they provide an experimental realization of the *XY* model; in particular, applying a magnetic field introduces frustration, measured by the flux per plaquette in units of the flux quantum.[1] The corresponding vortices induced by the field tend to form a regular flux lattice, thus lowering the free energy, and result in interplay with the underlying lattice periodicity. This gives rise to commensurate-incommensurate effects and leads to a rich variety of physics, including first-order and double transitions, reentrance, glassy behavior, quantum transitions, topological quantization, dynamic transitions, and resonance, etc.[2,3] In these phenomena vortex configurations and dynamics play crucial roles, driving transitions and governing transport properties. Here, one interesting question arises when an extra vortex is added into the system. While the vortex in general sits on a plaquette with minimum energy, which is separated by the potential barrier set by the underlying lattice structure, it may be driven into motion by applying currents, as it is exerted by the "Lorentz force" in the transverse direction, and accordingly generates nonvanishing voltage. Indeed, the voltage measurement in recent dynamic simulations,[4] performed in the presence of external currents, has given the pinning energy barriers as well as the critical currents, which agree fully with experimental results,[5] thus resolving the longstanding discrepancy in the frustrated case.

This paper focuses on the vortex dynamics in ladders of Josephson junctions, which provides the simplest system for probing the frustration effects: Those studied in existing literature include the vortex configuration and the critical current, depending on the frustration,[6,7] the vortex-vortex interaction decaying exponentially,[8] quantum effects,[9] and resonance.[10] Note the vast difference from the 2D system, especially in the vortex interaction, which is expected to affect significantly the dynamics of a vortex in a background of other vortices, i.e., in a frustrated system. In particular, domain walls in a ladder system assume the simple form of point defects, the dynamics of which is convenient to probe. We thus consider the domain wall defects created by adding an extra vortex in a fully frustrated ladder and examine their motion driven by external currents. In small systems, the symmetry argument and topological constraints allow one to compute analytically the energy barrier. More generally, the defect motion, driven by uniform currents, is investigated by means of dynamical simulations performed directly on the equations of motion. The resulting value of the energy barrier is found consistent with the analytical one obtained for small systems. Also observed is the defect motion, either sequential or simultaneous, depending on the size and the initial configuration. Such characteristics are attributed to the distance-dependent interaction between defects and the underlying lattice geometry.

There are five sections in this paper: Sec. II introduces the model system, whereas Sec. III is devoted to the analytical calculations of the energy barrier to the defect motion in small systems. In Sec. IV, we describe the numerical simulations performed on the equations of motion in the presence of uniform driving currents, and present the results. The current-voltage (*IV*) characteristics and the energy function are computed, which in turn give the critical current and the pinning energy barrier for various system sizes. Finally, a brief summary is given in Sec. V.

II. MODEL SYSTEM

We consider a ladder of Josephson junctions made of $2L$ superconducting grains weakly coupled to their nearest neighbors, the schematic diagram of which is shown in Fig. 1. The grains are located at sites $i \equiv (x,y)$, where x runs from 1 to L (in the leg direction) and the label $y(=1,2)$ describes, respectively, the lower and upper legs of the ladder. Each grain is characterized by the local condensed wave function or the order parameter

$$\Psi_i = |\Psi_i| e^{i\phi_i}, \tag{1}$$

where the local superconducting fluid density $|\Psi_i|$ is assumed to be constant at low temperatures. Accordingly, relevant fluctuations come from the phases ϕ_i and the Hamiltonian of the system in the presence of the external field is simply given by the sum of the nearest neighboring pair energies

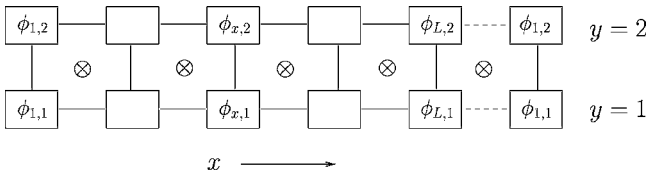

FIG. 1. Schematic notation for a Josephson-junction ladder. Each superconducting grain, denoted by a square, is characterized by the phase $\phi_{x,y}$ of the superconducting order parameter. The symbol $\otimes$ denotes the flux per plaquette from an external transverse magnetic field. The extra plaquette on the right-hand side represents the periodic boundary conditions.

$$H = -E_J \sum_{\langle i,j \rangle} \cos(\phi_i - \phi_j - A_{ij}), \tag{2}$$

where E_J is the coupling constant between the grains, $\langle i,j \rangle$ represents nearest neighboring pairs, and the bond angle A_{ij} is given by the line integral of the vector potential

$$A_{ij} = \frac{2\pi}{\Phi_0} \int_i^j \mathbf{A} \cdot d\mathbf{l} \tag{3}$$

with the flux quantum $\Phi_0 \equiv \pi\hbar c/e$. In the Landau gauge, the components of the vector potential $\mathbf{A}(x,y)$ are given by

$$A_x(x,y) = 0 \quad \text{and} \quad A_y(x,y) = \Phi x, \tag{4}$$

where Φ is the magnetic flux per plaquette and x is the position along the leg direction.

For the ladder in Fig. 1, the Hamiltonian reduces to

$$H = -E_J \sum_{x,y} \cos(\phi_{x,y} - \phi_{x+1,y}) - E_J \sum_x \cos(\phi_{x,1} - \phi_{x,2} - 2\pi f x), \tag{5}$$

where $f \equiv \Phi/\Phi_0$ measures the frustration of the system. In the fully frustrated case ($f=1/2$), which is our main concern in this work, every other site is occupied by a single vortex.

We now add or remove one vortex; this creates topological defects (domain walls) that affect the ground state. A typical vortex configuration in this case is displayed in Fig. 2. The extra vortex can move through the periodic potential produced by the lattice structure when it is subject to a perpendicular current. An estimation of the corresponding lattice pinning barrier is then made each time this extra vortex crosses the barrier. Note that the periodic potential is, in general, modulated significantly by other (underlying) vortices present in the system with $f=1/2$, resulting in a barrier strikingly different from that in the unfrustrated system ($f=0$).

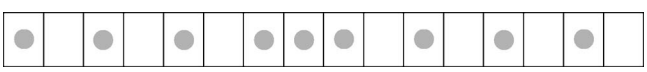

FIG. 2. Vortex configuration in the presence of an extra vortex in the fully frustrated ladder of size $L=16$. Filled circles represent vortices.

III. ANALYTIC CALCULATIONS

For convenience, we choose new gauge invariant phases that simplify the Hamiltonian and the current distribution in the system. Let θ_x and φ_x denote the following phase differences between the grains:

$$\theta_x = \phi_{x+1,1} - \phi_{x,1}$$

$$\theta'_x = \phi_{x+1,2} - \phi_{x,2}$$

$$\varphi_x = \phi_{x,1} - \phi_{x,2} - 2\pi f x. \tag{6}$$

It is easy to see, by symmetry and energy considerations, that the phase differences θ_x and θ'_x are opposite to each other.[6] Indeed, the sum of these phases around each plaquette is constrained topologically by the flux or frustration f and the (integer) vortex number n_x

$$\theta_x - \theta'_x - \varphi_{x+1} + \varphi_x = 2\pi(n_x - f) \equiv 2\pi q_x, \tag{7}$$

where q_x is the (fractional) vortex charge, and the Hamiltonian simply reads

$$H = -E_J \sum_x [\cos\theta_x + \cos\theta'_x + \cos\varphi_x] = -E_J \sum_x \left\{ 2\cos\left[\frac{\varphi_{x+1} - \varphi_x}{2} + \pi(n_x - f) \right] \times \cos\left(\frac{\theta_x + \theta'_x}{2} \right) + \cos\varphi_x \right\}. \tag{8}$$

Then the condition $\theta'_x = -\theta_x$ decouples the phases between the transverse directions and leads to a solution that minimizes this Hamiltonian. Using the current conservation laws, we can write a set of L equations for θ_x and φ_x at every node of the lattice

$$\sin\theta_x = \sin\theta_{x+1} - \sin\varphi_{x+1}, \tag{9}$$

with the boundary conditions

$$\theta_{x+L} = \theta_x \quad \text{and} \quad \varphi_{x+L} = \varphi_x. \tag{10}$$

The barrier energy E_B for a vortex moving along a ladder can be computed exactly on one simple example. In Fig. 3, we consider two plaquettes under closed boundary conditions and a single vortex in the system. In the notation of Fig. 3, the equations for the phases $(\theta, \theta', \varphi)$ in case (a) are given by

$$3\theta - \varphi = \pi$$

$$3\theta' + \varphi = -\pi$$

$$\sin\theta' = \sin\theta + \sin\varphi, \tag{11}$$

which yields $\theta = -\theta' = (\pi + \varphi)/3$. As a function of φ, the energy

$$E(\varphi) = -6\cos\left(\frac{\pi + \varphi}{3} \right) - \cos\varphi \tag{12}$$

has an absolute minimum for $\varphi = -\pi/2$, which in turn leads to $\theta = \pi/6$ and $E = -3\sqrt{3} \approx -5.196$, and a maximum for $\varphi =$

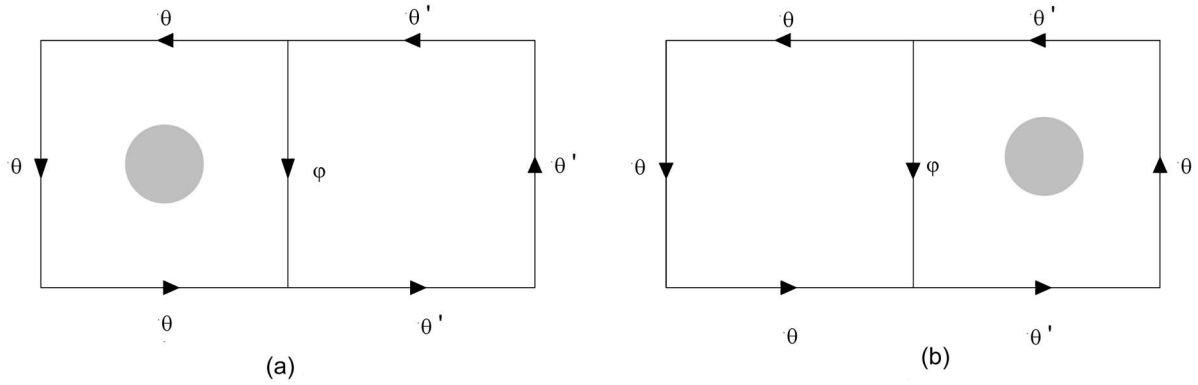

FIG. 3. Configuration of a two-plaquette system, with the phase difference labeled along each link. Filled circles represent vortices.

$-\pi$ together with $\theta=0$ and $E=-5$. On the other hand, in case (b), we have

$$3\theta - \varphi = -\pi$$

$$3\theta' + \varphi = \pi$$

$$\sin\theta' = \sin\theta + \sin\varphi, \tag{13}$$

the solutions of which are $\varphi=\pi/2$ and $\theta=-\pi/6$ for the ground state (with $E=-3\sqrt{3}$), and $\varphi=\pi$ and $\theta=0$ for the excited state (with $E=-5$). The excited states in both cases are equivalent since $\varphi=-\pi=\pi(\mathrm{mod}\,2\pi)$. This corresponds to the situation that the system evolves from configuration (a) to (b), namely, the instant when the vortex is exactly on the rung between the two plaquettes. Accordingly, the energy barrier is simply given by

$$E_B = 3\sqrt{3} - 5 \approx 0.196. \tag{14}$$

In the general case, the value $\varphi=\pi$ (or $-\pi$) in the excited state does not depend on the frustration parameter f since it is always a solution of the equation $\partial E(\varphi)/\partial\varphi=0$ with

$$E(\varphi) = -3\cos\left(\frac{2\pi f+\varphi}{3}\right) - 3\cos\left[\frac{2\pi(1-f)+\varphi}{3}\right] - \cos\varphi. \tag{15}$$

In the following, we accept that $\varphi=\pi$ corresponds to the solution of the excited state in which the vortex is on the rung for any given L; this will be checked numerically (see Fig. 6 below).

In a more complicated case, we consider a system with $L=8$ plaquettes. Figure 4 shows the phase configuration of an eight-plaquette system at $f=1/2$ under periodic boundary conditions, in the presence of an extra vortex. We consider

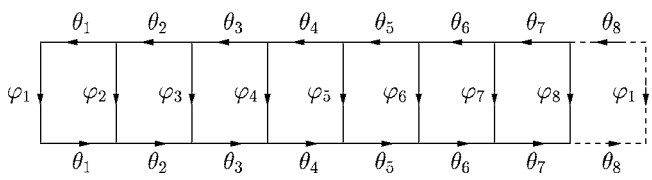

FIG. 4. Phase configuration of a Josephson-junction ladder of $L=8$ plaquettes. Periodic boundary conditions are employed.

three possible configurations (I, G, M) shown in Fig. 5, where filled circles and crosses represent vortices and defects (domain walls), respectively. Starting from the initial state I and driven by the injected current along the y direction, the system evolves eventually to configuration G via a number of intermediate configurations. It subsequently evolves to M and back to G. Configurations G and M correspond to the lowest-energy state and the high-energy (excited) state, respectively, and this evolution pattern repeats with time, which has been verified by extensive numerical simulations.

In the initial configuration I, the stationary phase relations are given by

$$2\theta_1 - \varphi_2 + \varphi_1 = -\pi, \quad 2\theta_2 - \varphi_3 + \varphi_2 = \pi$$

$$2\theta_3 - \varphi_4 + \varphi_3 = -\pi, \quad 2\theta_4 - \varphi_5 + \varphi_4 = \pi$$

$$2\theta_5 - \varphi_6 + \varphi_5 = -\pi, \quad 2\theta_6 - \varphi_7 + \varphi_6 = \pi$$

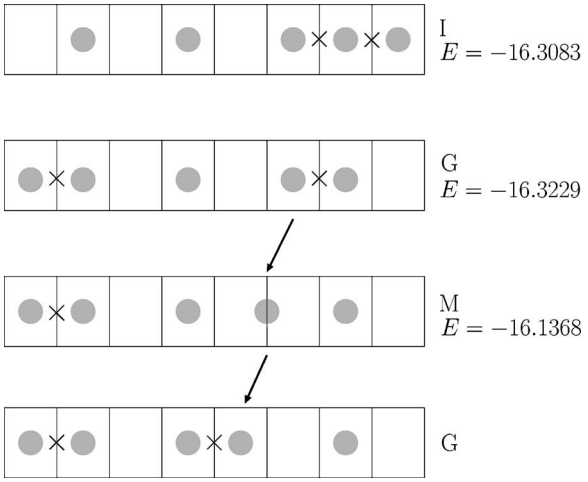

FIG. 5. Three vortex configurations (I, G, M), showing the presence of vortices (denoted by filled circles) and domain wall defects (denoted by crosses). Also shown is the estimated energy (in units of E_J) of each configuration. Arrows represent the time evolution of the configuration, which has been verified by extensive numerical simulations.

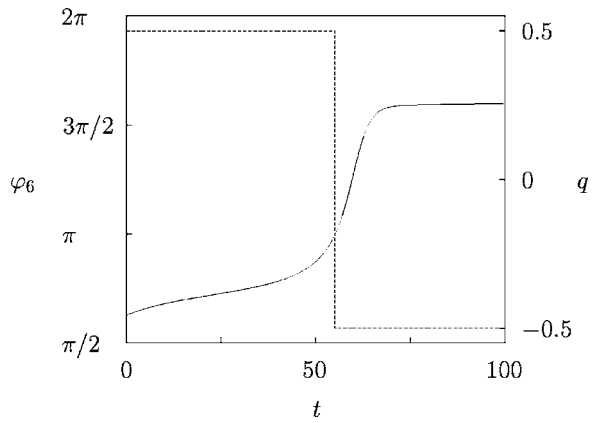

FIG. 6. Time evolution of the phase difference φ_6 across the rung (solid line, left vertical axis), together with that of the vortex charge $q=n-f$ on the plaquette just right of the rung (dotted line, right vertical axis). Time t is given in units of $\hbar/2ei_cR$.

$$2\theta_7 - \varphi_8 + \varphi_7 = \pi, \quad 2\theta_8 - \varphi_1 + \varphi_8 = \pi. \tag{16}$$

In units of the Josephson coupling energy E_J, the energy is estimated to be $E(I)=-16.3083$. For configuration G, the phase relations read

$$2\theta_1 - \phi_2 + \varphi_1 = \pi, \quad 2\theta_2 - \varphi_3 + \varphi_2 = \pi$$

$$2\theta_3 - \phi_4 + \varphi_3 = -\pi, \quad 2\theta_4 - \varphi_5 + \varphi_4 = \pi$$

$$2\theta_5 - \phi_6 + \varphi_5 = -\pi, \quad 2\theta_6 - \varphi_7 + \varphi_6 = \pi$$

$$2\theta_7 - \phi_8 + \varphi_7 = \pi, \quad 2\theta_8 - \varphi_1 + \varphi_8 = -\pi, \tag{17}$$

which yields the energy $E(G)=-16.3229$.

Configuration M describes an intermediate state via which the system goes from the state with the occupation number $(n_5=0,n_6=1)$ to that with $(n_5=1,n_6=0)$, namely, the vortex moves to the left by one plaquette, similarly to the evolution from (b) to (a) in Fig. 3. In this case, the vortex numbers in both cells are not well defined, but the vortex is said to be "spread" between the two plaquettes. To apply Eq. (9), we further take the two plaquettes on both sides of the rung as one unit cell. Since the net vortex charge enclosed in this cell (consisting of the two plaquettes) is zero, the sum of phase differences around it also vanishes. We thus have the condition $2\theta_5+\varphi_5+2\theta_6-\varphi_7=2\pi(n_5-f+n_6-f)=0$, with $n_5+n_6=1$. The remaining relations are given by

$$2\theta_1 - \varphi_2 + \varphi_1 = \pi, \quad 2\theta_2 - \varphi_3 + \varphi_2 = \pi$$

$$2\theta_3 - \varphi_4 + \varphi_3 = -\pi, \quad 2\theta_4 - \varphi_5 + \varphi_4 = \pi,$$

$$2\theta_7 - \varphi_8 + \varphi_7 = \pi \quad 2\theta_8 - \varphi_1 + \varphi_8 = -\pi. \tag{18}$$

As already addressed, the vortex sits on the rung in this configuration and the phases take the radial direction around the center of the rung, thus leading to the phase difference $\varphi_6=\pi$ along the rung. This is manifested by the time evolution of φ_6, as shown in the next section (see Fig. 6). We thus set $\varphi_6=\pi$ and obtain the energy of the configuration: $E(M)=-16.1368$.

Together with the result of $E(G)$, we estimate the pinning barrier according to

$$E_B \equiv E(M) - E(G) = 0.1861. \tag{19}$$

Note that this value, obtained for $L=8$, is lower than the value 0.19615 in the two-plaquette case $(L=2)$. We thus expect that the energy barrier E_B in the thermodynamic limit $(L\to\infty)$ has a value still lower than 0.1861.

IV. NUMERICAL SIMULATIONS

To evaluate the precise value of the energy barrier for various system sizes, we have performed extensive dynamic simulations on the resistively shunted junction (RSJ) model. The dynamics of the RSJ model, with single-junction critical current i_c, and shunt resistance R, is governed by the set of equations of motion for the phase ϕ_i,

$$\sum_j{}' \left[\frac{\hbar}{2eR}\frac{d\tilde{\phi}_{ij}}{dt} + i_c \sin\tilde{\phi}_{ij} \right] = I_i, \tag{20}$$

where $\tilde{\phi}_{ij} \equiv \phi_i - \phi_j - A_{ij}$ is the gauge-invariant phase difference across the junction (ij), and the primed summation runs over the nearest neighbors of grain i. The system is driven by the current $I_i=I_{x,y}=I(\delta_{y,2}-\delta_{y,1})$ (applied to grain i), namely, uniform current I is injected to and extracted from each grain on the upper $(y=2)$ and lower $(y=1)$ legs, respectively. Using a modified Euler method, we have integrated Eq. (20) with the time step of size $\Delta t=0.05$ (in units of $\hbar/2ei_cR$) for a variety of ladders up to the system size $L=512$. In addition to the periodic boundary conditions imposed along the x direction, we introduce a 2π phase slip across the whole system:

$$\phi_{L+1,2} = \phi_{1,2} + \pi$$

$$\phi_{L+1,1} = \phi_{1,1} - \pi, \tag{21}$$

which generates a single extra vortex.

We first examine how the rung phase difference φ_6 varies in the vortex motion and plot in Fig. 6 its time evolution in the system of eight plaquettes. Also plotted is the evolution of the vortex charge $q=n-f$ (with n being the vortex number) on the plaquette just right of the rung. It is observed that q (or n) changes rather abruptly from $1/2$ to $-1/2$ (or from 1 to 0), describing the motion of a vortex to the left. In particular, at the moment of the change, i.e., when the vortex is located *on* the rung, the phase difference φ_6 indeed has the value π, as expected.

Figure 7 shows typical motion of defects under the driving currents. At first, two defects (i.e., two domain walls separating the three neighboring vortices) are next to each other, as shown in the first configuration (from top to bottom). The distance between the domain wall defects grows with time until this distance eventually becomes half the system size (see the second configuration). Then, the defect on the right moves first (changing the configuration to the third

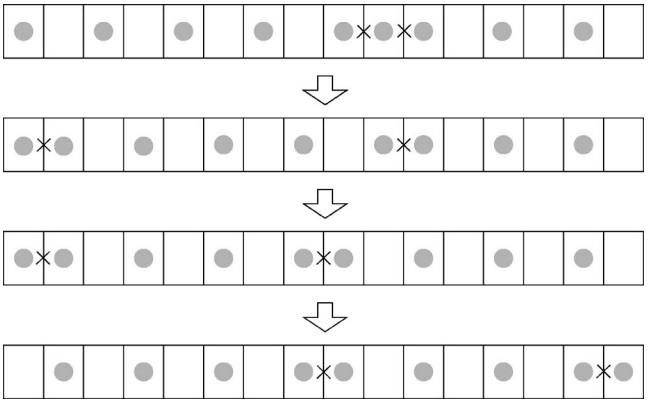

FIG. 7. Pattern of defect motion in a fully frustrated ladder ($f=1/2$), with filled circles and crosses denoting vortices and domain walls, respectively, as time goes by (in the direction of the arrows). Currents are applied uniformly along the rungs.

one), subsequently followed by the motion of the one on the left (resulting in the fourth configuration). In the case that there are only a few plaquettes ($L<40$), this behavior is always observed, regardless of the initial distance between the two defects. On the other hand, in a system of larger size, two types of behavior are observed, depending on initial conditions. When the two defects are initially located at nearby sites, they move simultaneously through transient states and the distance between them does not grow beyond 20 plaquettes. In contrast, two defects distant by more than 20 plaquettes tend to move sequentially for appropriate initial phase configurations. We presume that such size dependence has its origin in the interaction between defects and the underlying periodic lattice geometry. Namely, the interaction between two domain wall defects becomes vanishingly small as the distance is increased beyond 20 plaquettes, which may reflect the exponentially decaying interaction between vortices.[8] In this manner, the characteristic interaction between domain walls in a background of vortices appears to be exposed.

In order to estimate the pinning barrier, we compute the *IV* characteristics and the critical current I_c, and probe their behaviors with the system size L. The voltage across the system is given by the ac Josephson relation[11]

$$\langle V\rangle = \frac{\hbar}{2eL}\left\langle \sum_x \frac{d(\phi_{x,2}-\phi_{x,1})}{dt}\right\rangle \tag{22}$$

and the resulting characteristics are displayed in Fig. 8 for system size $L=8$, 16, and 24. Systems larger than $L=24$ turn out to exhibit the same *IV* characteristics as the case $L=24$ and are thus not shown here. It is observed that nonzero voltage develops as the driving current I is increased beyond a certain value. The size dependence of the corresponding critical current I_c is plotted in the inset of Fig. 8, which demonstrates that I_c first reduces with the system size L and saturates to a nearly constant value beyond $L=24$. In the thermodynamic limit, I_c is shown to approach the value 0.089 (in units of the single-junction critical current i_c); this

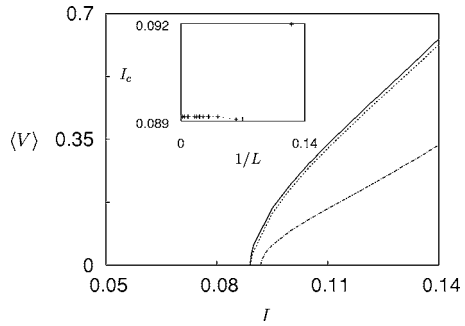

FIG. 8. *IV* characteristics for the system size $L=8$, 16, and 24, respectively, from bottom to top. The inset shows the critical current I_c as a function of L. Current I and voltage V are expressed in units of i_c and i_cR, respectively.

is close to the value $I_c\approx 0.1$ at $f=1/2$, extracted roughly from Fig. 1(a) of Ref. 7.

In Fig. 9, we display the typical time dependence of the energy $E(t)$. With the driving current $I=I_c(L)+0.0001$ just above the critical value, the energy is calculated through the use of Eq. (5). Note in Fig. 9 that (a) and (b) correspond to the sequential motion of defects for the system size $L=8$ (smaller than 40) and 64 (larger than 40), respectively. As the defect moves across one plaquette, $E(t)$ goes through a maximum corresponding to the excited state discussed in Sec. III. The lowest-energy state corresponds to configuration G and the maximum one to M shown in Fig. 5. As pointed out, the defects can move simultaneously for appropriate initial conditions. Such simultaneous motion is indeed observed in Fig. 9(c), which reveals the doubling of both the amplitude and the period of $E(t)$ (i.e., the energy barrier and the period of the defect motion). The two transient states seen in the inset of Fig. 9(c) indicate that the system possessing two defects is not completely coherent in the first stage of the dynamics.

The pinning energy barrier E_B, defined to be the difference between the maximum energy $E(M)$ and the minimum one $E(G)$, is thus computed as the system size is varied. The size dependence of E_B is then examined and shown in Fig. 10 for sequential and simultaneous motion of defects. In the former case, the energy barrier is observed to approach the value

$$E_B = 0.1827$$

in the thermodynamic limit. This value is slightly below the one found analytically in the eight-plaquette system, as expected. In the case of simultaneous motion, Fig. 10(b) shows that the energy barrier becomes double for the system size $L>40$.

V. SUMMARY

We have studied the dynamics of domain wall defects created by adding an extra vortex in a fully frustrated Josephson-junction ladder. The defects are, in general, pinned by the energy barrier generated by the underlying lattice structure and other vortices induced by an external magnetic field or frustration. Making use of the symmetry

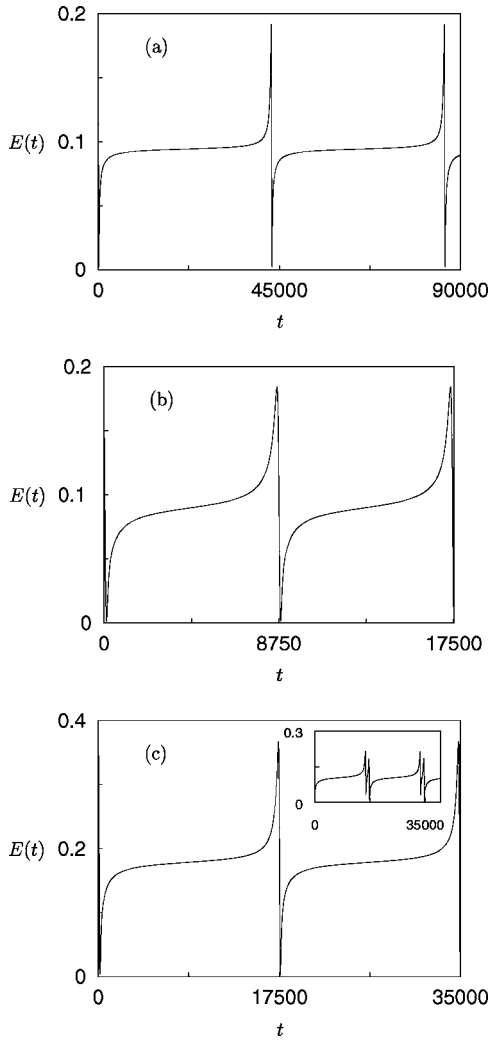

FIG. 9. Time evolution of energy $E(t)$ in systems of size $L=8$ (a) and 64 [(b) and (c)]. The uniform driving current $I=I_c(L)+0.0001$ has been applied along each rung. (a) and (b) describe the *sequential* motion while (c) corresponds to the *simultaneous* motion (see the text). For convenience, $E(t)$, given in units of E_J, has been shifted such that $E=0$ corresponds to the minimum. The inset in (c) shows a transient behavior: The two peaks eventually merge into the one peak shown in the main plate.

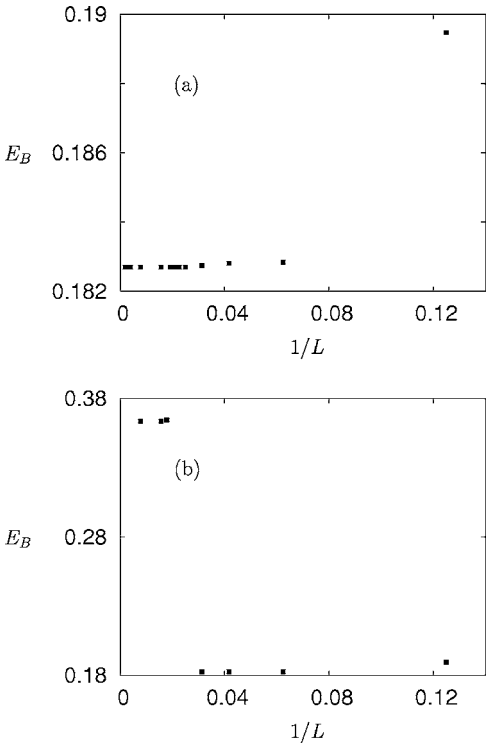

FIG. 10. Pinning energy barrier E_B (in units of E_J) as a function of the system size L. Energy barriers corresponding to (a) sequential and (b) simultaneous motion of defects are displayed.

and topological constraints, we have computed the energy barrier E_B in systems of size $L \leqslant 8$. The defects may be put to motion by applying currents larger than the critical current. The corresponding motion in the system, driven by uniform currents just above the critical value, has been investigated by means of dynamical simulations performed directly on the equations of motion. The resulting numerical estimation of $E_B=0.1827$ (in units of the Josephson coupling energy) is fully consistent with the analytical value obtained from resolution of the phases in the eight-plaquette ($L=8$) system. In the dynamical study of the system, we have also observed that the defects move sequentially in small systems ($L<40$). On the other hand, in larger systems, the domain walls may also display coherent motion, namely, they can move simultaneously as well as sequentially, depending on the initial configurations. Such difference has been attributed to the distance-dependent interaction between defects and the underlying lattice geometry.

ACKNOWLEDGMENTS

One of us (M.Y.C.) acknowledges the visitor grant from the CNRS, France and thanks the Laboratoire de Physique Théorique, Strasbourg, for its kind hospitality during his stay. H.K. thanks Kyuho Lee for help in obtaining numerical solutions. This work was supported in part by the Korea Science and Engineering Foundation through National Core Research Center for Systems Bio-dynamics and by the Ministry of Education of Korea through the BK21 program.

[1] S. Teitel and C. Jayaprakash, Phys. Rev. B **27**, R598 (1983); M. Y. Choi and S. Doniach, *ibid.* **31**, 4516 (1985); W.-Y. Shih and D. Stroud, *ibid.* **32**, 158 (1985).

[2] For a review, see, e.g., B. J. Kim, G. S. Jeon, and M. Y. Choi, in *High-Temperature Superconductors, Vol. 39: Studies of Josephson Junction Arrays*, edited by A. V. Narlikar (Nova, New York, 2001), pp. 245–267.

[3] For some recent works on dynamics, see G. S. Jeon, J. S. Lim, H. J. Kim, and M. Y. Choi, Phys. Rev. B **66**, 024511 (2002); G. S. Jeon, S. J. Lee, and M. Y. Choi, *ibid.* **67**, 014501 (2003); J. S. Lim, M. Y. Choi, J. Choi, and B. J. Kim, *ibid.* **69**, 220504(R) (2004).

[4] J. S. Lim, M. Y. Choi, B. J. Kim, and J. Choi, Phys. Rev. B **71**, 100505(R) (2005).

[5] M. S. Rzchowski, S. P. Benz, M. Tinkham, and C. J. Lobb, Phys. Rev. B **42**, 2041 (1990); S. P. Benz, M. S. Rzchowski, M. Tinkham, and C. J. Lobb, *ibid.* **42**, 6165 (1990).

[6] J. J. Mazo, F. Falo, and L. M. Floría, Phys. Rev. B **52**, 10433 (1995); C. Denniston and C. Tang, Phys. Rev. Lett. **75**, 3930 (1995).

[7] I.-J. Hwang, S. Ryu, and D. Stroud, Phys. Rev. B **53**, R506 (1996); M. Barahona, S. H. Strogatz, and T. P. Orlando, *ibid.* **57**, 1181 (1998).

[8] S. Kim, Phys. Lett. A **229**, 190 (1997); J. Yi, S.-I. Lee, and S. Kim, Phys. Rev. B **63**, 132501 (2001).

[9] M. Kardar, Phys. Rev. B **33**, 3125 (1986). M. Lee, M.-S. Choi, and M. Y. Choi, *ibid.* **68**, 144506 (2003).

[10] B. J. Kim, M.-S. Choi, P. Minnhagen, G. S. Jeon, H. J. Kim, and M. Y. Choi, Phys. Rev. B **63**, 104506 (2001); G. S. Jeon and M. Y. Choi, *ibid.* **66**, 064514 (2002).

[11] See, e.g., M. Tinkham, *Introduction to Superconductivity*, 2nd ed. (McGraw-Hill, New York, 1995).